Photoacoustics 41 (2025) 100664

Contents lists available at ScienceDirect

Photoacoustics

journal homepage: www.elsevier.com/locate/pacs

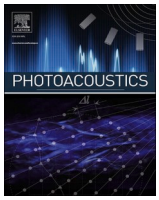

No document header

Monitoring of microvascular calcification by time-resolved photoacoustic microscopy

Haigang Ma [a,b,c,*], Yinshi Yu [a,b,c], Yahui Zhu [a,b,c], Hongjun Wu [a,b,c], Haixia Qiu [d], Ying Gu [d], Qian Chen [a,c], Chao Zuo [a,b,c,*]

[a] Smart Computational Imaging Laboratory (SCILab), School of Electronic and Optical Engineering, Nanjing University of Science and Technology, Nanjing, Jiangsu 210094, China
[b] Smart Computational Imaging Research Institute (SCIRI) of Nanjing University of Science and Technology, Nanjing, Jiangsu 210019, China
[c] Jiangsu Key Laboratory of Spectral Imaging & Intelligent Sense, Nanjing, Jiangsu 210094, China
[d] Department of Laser medicine, the First Medical Center of PLA General Hospital, Beijing 100853, China

ARTICLE INFO

Keywords:
Photoacoustic microscopy
Microvascular calcification
Bio-elastic monitoring
Bio-mechanical assessment

ABSTRACT

Monitoring of microvascular calcification (MC) is essential for the understanding of pathophysiological processes and the characterization of certain physiological states such as drug abuse, metabolic abnormality, and chronic nephrosis. In this work, we develop a novel and effective time-resolved photoacoustic microscopy (TR-PAM) technology, which can observe the obvious microvascular bio-elastic change in the development process of the MC owing to the calcium deposition along vascular walls.The feasibility of the TR-PAM imaging was validated using a group of agar phantoms and *ex vivo* tissues. Furthermore, MC pathological animal models were constructed and imaged *in situ* and *in vivo* by the TR-PAM to demonstrate its capability for the bio-mechanical monitoring and characterization of MC, and experimental results were consistent with the pathological knowledge. The feasibility study of monitoring MC by the TR-PAM proves that this technique has potential to be developed as a superficial microvascular bio-mechanical assessment method to supplement current clinical strategy for prediction and monitoring of some diseases.

1. Introduction

Vascular calcification (VC) is a complex disorder that affects both major and minor blood vessels, primarily characterized by the deposition of calcium along the vascular walls [1–3]. This calcification typically results in vascular sclerosis and reduced compliance, which are significantly correlated with increased cardiovascular mortality [3]. VC is particularly prevalent in the chronic kidney disease (CKD) population, where its frequency rises with the progression of CKD [4]. Additionally, VC is recognized as a clear indicator of atherosclerosis and is strongly linked to diabetes, dyslipidemia, and hypertension [3,5]. Despite its significance, most scientific research and clinical screening for VC focus primarily on cardiovascular and carotid arteries, as well as other major blood vessels [3]. While monitoring VC in these vessels can directly reflect the status of related diseases, the techniques involved are complex, costly, and challenging to apply for long-term monitoring. Superficial microcirculation serves as a marker of generalized microvascular dysfunction in cardiovascular and metabolic diseases. Indeed, past research has associated these symptoms with calcified arterioles, capillaries, and venules [6], and microvascular calcification (MC) has long been recognized as a major complication of CKD and diabetes [6–8]. Therefore, the use of effective biomedical imaging technology to monitor MC in soft tissues is crucial for revealing the development of adverse microvascular events. This approach is also of great significance for the clinical screening, prevention, treatment, and prognosis evaluation of cardiovascular and metabolic diseases. Commonly used methods for the evaluation of vascular calcification (VC) include radiography [9], computed tomography (CT) [10], and others. However, these methods are unsuitable for long-term monitoring and early screening of microvascular calcification (MC) in superficial soft tissues due to radiation exposure. The mechanical properties of microvascular structures provide extensive physiological and pathological information about calcification, which changes as MC progresses; therefore, quantifying microvascular mechanical parameters offers a practical and effective

* Corresponding authors at: Smart Computational Imaging Laboratory (SCILab), School of Electronic and Optical Engineering, Nanjing University of Science and Technology, Nanjing, Jiangsu 210094, China.
E-mail addresses: mahaigang@njust.edu.cn (H. Ma), zuochao@njust.edu.cn (C. Zuo).

https://doi.org/10.1016/j.pacs.2024.100664
Received 24 August 2024; Received in revised form 5 November 2024; Accepted 5 November 2024
Available online 7 November 2024

approach for the evaluation and monitoring of MC [11,12]. Many techniques have been proposed to measure vascular-scale mechanical properties, especially elasticity (i.e., Young's modulus). Traditional elastography techniques, such as ultrasound elastography (USE) [13] and magnetic resonance elastography (MRE) [14], have been widely used to investigate vascular elasticity in assessing diseases of the carotid artery, cardiovascular system, and peripheral arteries. While these techniques can measure elasticity over larger areas, their limited spatial resolution restricts the detailed mapping of elasticity in the microvascular system, particularly in capillaries. With its high spatial resolution, atomic force microscopy (AFM) has been used to estimate elasticity based on vascular deformation in response to an external load [15]. However, AFM is constrained by the imaging range, speed, probe quality (as probe performance and quality significantly impact the accuracy of test results), and the scanning image size of the individual probe. Furthermore, AFM requires contact with tissue to impose mechanical stress, which is not always desirable. Optical coherence elastography (OCE) evaluates elasticity through static compression or dynamic vibration within microvascular tissue [16]. However, the accuracy of elasticity estimation is insufficient for complex and imperceptible microvessels in heterogeneous soft tissues. Therefore, the non-invasive monitoring and evaluation of microvascular biomechanics at a micron-scale resolution and centimeter-scale regions over a long period remains a challenge for existing elastography techniques. In addition, the existing imaging modalities (namely, CT, USE, MRE, AFM, and OCE) for recovering elastic properties fail to provide physiological information about microvascular tissues [17].

As a rapidly developing non-invasive hybrid imaging technology, photoacoustic imaging (PAI) combines the advantages of rich optical absorption contrast and high acoustic penetration depth. It has several key benefits: (1) high spatial resolution and high contrast obtainable at penetration depths that are not achievable with commercially available high-resolution optical-based microscopic imaging modalities (including two-photon, confocal, and OCT); (2) high scalability of imaging, ranging from individual cells to the entire body; (3) the ability to obtain pathophysiological information through multispectral PAI, such as physiological states of tissues related to pathological stages by measuring functional parameters (Hb, HbO2, glucose, and lipids) that control physiological activities like metabolism, as well as genetic and molecular activities [17–21]. Although it may be possible to directly analyze the amount of calcium salts deposited on blood vessel walls using multispectral PAI, monitoring MC based on spectral information requires the application of spectral unmixing techniques to multispectral data. The spectral responses from different chromophores must be delineated using mathematical calculations from the PA images acquired with various excitation wavelengths. Therefore, this MC monitoring based on spectral information is very demanding on the laser, requiring lasers with multiple wavelengths as the PA excitation source (in general, the greater the number of excitation wavelengths, the higher the accuracy of detection). Additionally, complex spectral unmixing operations render PA imaging systems more expensive. Furthermore, the proportion of blood components (for example, Hb, HbO2, glucose, water, and other minerals) is easily affected by changes in external factors (such as exercise, temperature, and diet), which can lead to lower accuracy and sensitivity in the analysis and detection of calcium salt deposition using this MC monitoring method based on spectral information.

In PAI modality, a highly energetic optical beam is adapted to irradiate target sample of interest over a prespecified region (using a short-laser pulse in nanoseconds), and then the resulted initial pressure rise is selectively detected by employing a tightly focusing ultrasonic detector, that is, it is converted into photoacoustic (PA) signal [22–24]. As mechanical waves, the produced PA signal naturally carries mechanical information of the excited target, enabling PAI to be a promising strategy for vascular bio-mechanical characterization, especially in measurements of vascular elasticity, and subsequently for the evaluation of MC [17,25].

There have been several PA studies on measuring the elastic properties of biological tissue. For example, the Young's modulus of in vivo human skeletal muscle was quantified by implementing quantitative PA elastography [26,27]. However, the methods face challenges when surveying irregular objects due to the necessity of applying uniform external pressure to the target being measured [28]. Another method involves the development of PA elasticity imaging, which establishes a relationship between the PA phase delay and the elasticity of targets [29]. The technique has achieved multi-scale mappings of bio-elastic properties ranging from cells to organs without extrinsic mechanical loading and has also been successfully applied in pathological applications, such as cancer [30], hepatic fibrosis [31], atherosclerotic plaque [32], and brain diseases [33]. Additionally, the utilization of time and phase characteristics of the PA response enables PA elasticity imaging to investigate both the elastic and viscous moduli simultaneously at the tissue level [34]. Meanwhile, some related techniques have also been explored [35,36]. The PA resonance effect method relies on resonance responses at specific frequencies, making it susceptible to tissue heterogeneity and limiting its application in complex tissues. The ratiometric PA elastic oscillation method is sensitive to signal quality and noise, resulting in reduced stability in dynamic physiological environments, which makes it less suitable for long-term monitoring. Although these studies indicate that PAI has provided feasible approaches to measure the mechanical information of biological tissue, it is still in the developmental stage, and the interrogation of elastic properties of in situ microvascular tissue at the micrometer scale has not been realized, especially in the context of long-term monitoring and assessment of MC caused by drug abuse or metabolic diseases. Quantitative monitoring and assessment of MC (i.e., quantifying measurements) of elasticity and discriminating contrast in PA signals from elastic and other parameters (including optical absorption coefficient) remain challenges from a technological standpoint. Furthermore, despite the number of in vivo models, exploration to clarify the developmental process by which excess exogenous vitamin D or metabolic disturbances promote MC is still lacking. To address these pressing challenges, we develop a method based on the detection of laser-induced transient stress by a time-resolved photoacoustic microscopy (TR-PAM) technology, which was first used to extract the elastic properties for monitoring and assessment of MC in soft tissue. The TR-PAM can calculate elasticity moduli by utilizing the time characteristics of PA response, which does not track the wave propagation in the complex and heterogeneous soft tissue, but instead leverages the temporal response characteristics at the excitation microvascular of PA point source, allowing to obtain the retrieval of in situ mechanics of microvascular tissue. In addition, it does not need prior knowledge of the direction of wave propagation, on account of the PA wave is an omnidirectional elastic wave by volume expansion of microvascular tissue. More importantly, the time-resolved MC monitoring method mainly depends on the characteristics of vascular elastic changes, which is not easily affected by changes in components of blood. The interrogation of elastic properties of in situ microvascular tissue at micrometer resolution and large field coverage has been realized by the method, especially used in the long-term, repeated, and non-invasive monitoring and assessment of MC *in vivo*. In conclusion, the main motivation of the work is to develop a TR-PAM method to investigate the elastic moduli of microvessels at a micron-scale level *in vivo*, and can enable preliminary monitoring of the elastic parameters for development process of the MC related animal models of diseases.

Experiments in animal models reveal that TR-PAM technique enables effective monitoring of the elastic parameters for examinations of the MC related diseases. Firstly, utilizing the model of MC induced by injecting vitamin D3, mice ears' microvascular biomechanics distributions were observed from the reconstructed elasticity maps, and this implies that the clear development process of MC induced by excessive consumption of vitamin D3 can be monitored. Secondly, in the serial PA

elasto-gram of diabetic mice ears' micro vessels at different diseased stages can be clearly identified based on the elastic variations due to their differences in MC. Finally, the TR-PAM results were further registered and demonstrated by the model of CDK mice, and high correlation in their feature patterns of MC was observed. Taken together, these experiments in animal models suggest that the TR-PAM method supports micron-scale and tissue-level mappings of elastic properties in vivo, and can enable continuous monitoring of the elastic parameters for development process of the MC related excess exogenous vitamin D or metabolic diseases. The technology opens new perspectives for in situ time-resolved elasticity imaging and provides a great potential in biomechanics-parametric characterizing MC information.

2. Methodology

In this section, an elastic calculation method based on thermoelastic expansion is introduced, and then a bio-mechanical model is established, which can determine the elastic parameters by exploring the rise time characteristics of PA signals. Secondly, the TR-PAM system is set up for the assessment of MC in soft tissue. Finally, the preparation of agar phantom, *ex vivo* pork tissues, *in vivo* mice models and preparation of vascular calcification pathological sections are introduced.

2.1. Principle of monitoring-based MC by TR-PAM

The TR-PAM method is based on the principle of temporal stress confinement in the target sample. Here, the initial pressure generated in microvascular tissue, which is heated instantaneously by short laser pulses, is proportional to the absorbed laser energy density. Additionally, the exponential profile of the initial pressure distribution in the target microvascular tissue corresponds to the z-axis distribution of the absorbed laser fluence. More specifically, the time-to-peak displacement of the PA signal is inversely correlated with the bulk elastic modulus. A volume dataset can be obtained using a raster scanning technique, where a time-resolved measurement at each scanning position yields a one-dimensional PA signal.

According to the thermal expansion mechanism, the laser pulse irradiating the absorption region, such as the microvascular tissue, will cause local oscillation and produce PA pressure wave, as shown in Fig. 1 (a). Considering linear, isotropic and viscoelastic media, the Navier equation determines the displacement of the sample at each laser excitation point [34,37], as follows:

$$\rho\frac{\partial^2\boldsymbol{u}}{\partial t^2} = (\lambda+\mu)\nabla(\nabla\cdot\boldsymbol{u})+\mu\nabla^2\boldsymbol{u}+(\varepsilon+\eta_0/3)\frac{\partial}{\partial t}\nabla(\nabla\cdot\boldsymbol{u})+\eta_0\frac{\partial}{\partial t}\nabla^2\boldsymbol{u}+\boldsymbol{F} \tag{1}$$

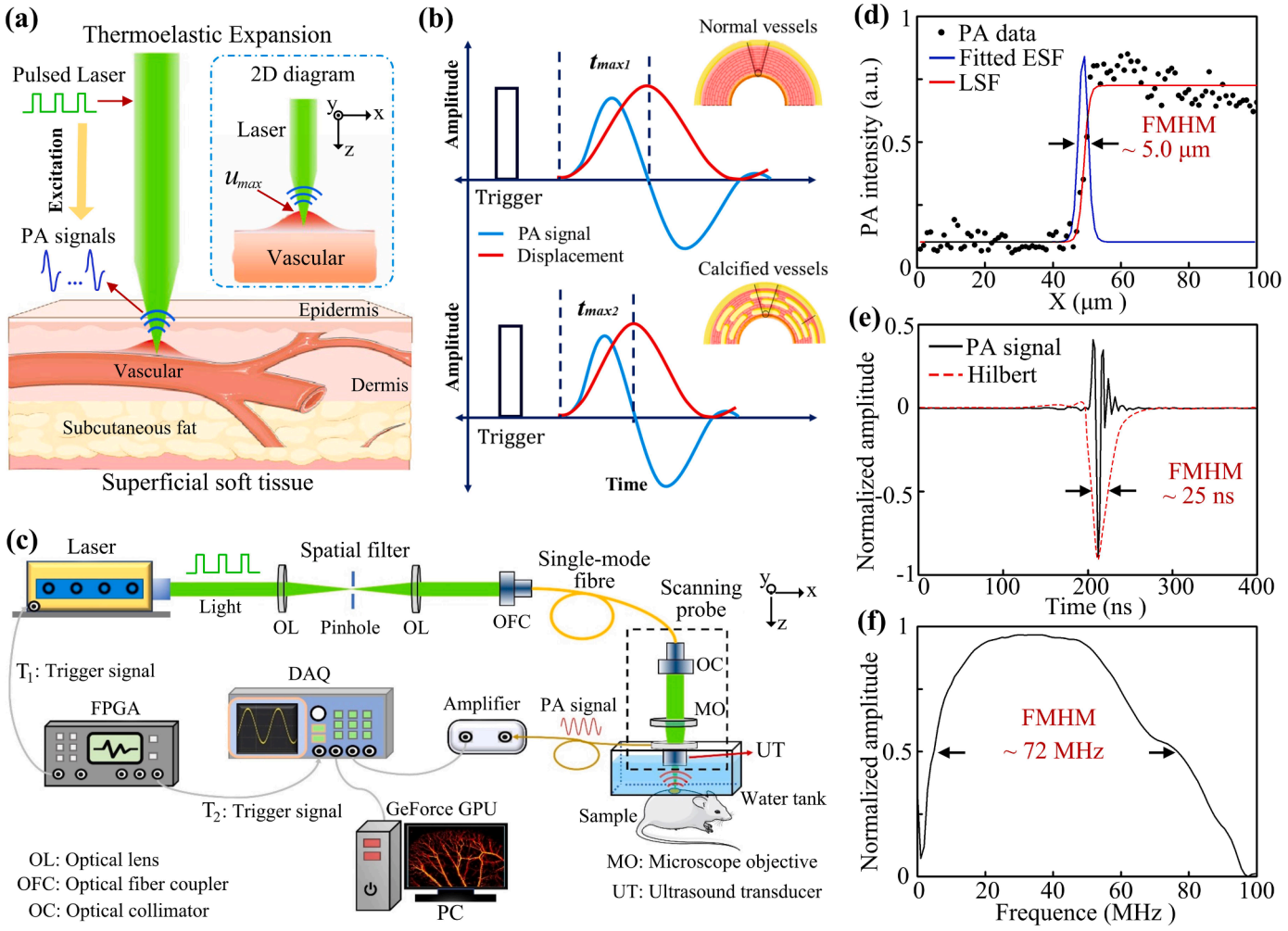

Fig. 1. Underlying principle of TR-PAM and theoretical prediction of PA response. (a) Laser-induced thermoelastic displacement ($\boldsymbol{u}$) and subsequent PA response based on the optical absorption-induced thermoelastic expansion for vascular tissues. (b) The principle of TR-PAM: elasticity and calcification estimations from vascular PA time response characteristic. (c) Experimental setup of the TR-PAM. (d) Distribution of the PA-normalized function value along the the sharpedged surgical blade indicated. (e) Pulse response of the transducer at the focus. (f) Amplitude frequency response of the transducer. DAQ: Data acquisition; FPGA: Field-programmable gate array.

Here, ρ is the mass density, $\boldsymbol{u}$ is the displacement vector, λ and μ are Lame constants, ε is the volume viscosity, η_0 is shear viscosity, and $\boldsymbol{F}$ is the equivalent excitation force induced by laser. According to the Helmholtz equation, the displacement vector $\boldsymbol{u}$ can be divided into P-wave u_p and S-wave u_s, and the two waves propagate independently in the medium. Since the S-wave $u_s$cannot travel through water, PA waves behave as P-waves u_p in water, i.e, $\nabla \times u_p = 0$. Simplifying the above equation gives:

$$\rho \frac{\partial^2 u_p}{\partial t^2} = F_{\text{exc}} + (\lambda + 2\mu)\nabla^2 u_p + (\varepsilon + 4/3\eta_0)\frac{\partial}{\partial t}\nabla^2 u_p \tag{2}$$

In Eq. (2), the term$\lambda + 2\mu$is denoted by the apparent elastic modulus E, and the term$\varepsilon + 4/(3\eta_0)$is denoted as apparent viscosityη. The excitation forceF_{exc}caused by a Gaussian laser beam is expressed as:

$$F_{exc} = \mu_a \Gamma P \Big/ c \cdot f(t) \cdot \exp[-\mu_a z - (r/R)^2] \tag{3}$$

Where μ_a is the light absorption coefficient, Γ is the Grüneisen parameter, P is the initial laser power density along the beam axis, c is the speed of light in a vacuum, $f(t)$describes the temporal dependence of the laser pulse, r is the radial coordinate, and R is the waist radius of the Grüneisen laser beam. Eq. (3) can be converted to

$$\frac{\partial^2 u_p}{\partial t^2} - \left(\frac{E}{\rho} + \frac{\eta}{\rho}\frac{\partial}{\partial t}\right)\nabla^2 u_p = \frac{\mu_a \Gamma P}{\rho c} f(t) \exp\left(-\mu_a z - \frac{r^2}{R^2}\right) \tag{4}$$

By using the Hankel transform method, the displacement$u_p$can be solved analytically at the focal region:

$$u_p = \frac{\sqrt{\pi}\mu_a \Gamma R P \tau}{2c\sqrt{\rho E}} \frac{\left(\frac{\sqrt{E/\rho}}{R}\right) t}{1 + \frac{2\eta}{\rho R^2} t + \left(\frac{\sqrt{E/\rho}}{R}\right)^2 t^2} \tag{5}$$

In Eq. (5),$\tau$is the laser pulse width, and the rise time $t_{\max}$of PA signal required for the displacement to reach the maximum$u_{\max}$at the focal region is related to the elastic modulus of the sample tissue. Therefore, the relation between the apparent elastic modulus E and the rise time $t_{\max}$ can be expressed as:

$$E = K\rho(R/t_{\max})^2 \tag{6}$$

Where K is the system constant, which is a fixed value in the same system. And the elastic modulus E is correlated with the density of the imaging sample, and rising time $t_{\max}$ of PA signal [33].

MC in soft tissue is the phenomenon of calcium salt deposition in the blood vessels of patients. Continuous deposition of calcium salt will lead to the fracture of vascular elastic fibers, and the response of blood vessels to external stress becomes more difficult, and the elastic modulus increases [11,37]. The relationship between the degree of MC (D_{MC}) and the elastic modulus E can be expressed as:

$$D_{MC} \propto E \propto \frac{\rho R^2}{(t_{\max})^2} \tag{7}$$

Here, the higher the value D_{MC}, the higher the degree of MC, and the blood vessels are less likely to deform. When MC occurs, the elastic modulus E increases, and the rise time $t_{\max}$ of PA signal decreases, as shown in Fig. 1(b). Therefore, the elastic modulus E and the degree of MC (D_M) can be estimated by extracting the rise time $t_{\max}$ of PA signal.

2.2. TR-PAM system

The schematic diagram of the TR-PAM system is shown in Fig. 1(c). The TR-PAM system employs a nanosecond laser system operating at 532 nm with a pulse width of 25 ns. The laser beam is attenuated, spatially filtered, and coupled to an optical fiber as the excitation source. It is then cleaned by a spatial filter system, passing through a 10-μm -diameter pinhole for spatial filtering, and subsequently coupled into a single-mode fiber by a fiber coupler. The single-mode fiber guides the laser beams into a PA probe with a microscope objective (MPlan Apo HL, 5X/0.13, Sigma), a ringed focused ultrasonic transducer (40S1F8, Doppler Inc.), and a 2D scanner. The transducer has a central frequency (-6 dB) of 40 MHz, a focal length of 8 mm, a relative bandwidth (-6 dB) of 72 MHz, and a peak-to-peak sensitivity of −45 dB, which is used to detect PA signals. In this context, the tightly focusing nature of the transducer enables it to detect PA signals over a narrow region specified by its focal zone (focal spot size ~50 μm). To ensure optimal detection sensitivity, the focal points of the laser and transducer are configured coaxially and adjusted to the same depth position. The detected signals are amplified (LNA-650, RF Bay) and digitized with a data acquisition card (M4i.4450-x8, Spectrum) at a sampling rate of 400 MS/s. When the field-programmable gate array (FPGA) receives a pulse signal from the 2D scanner, it simultaneously generates two trigger signals, T_1 and T_2, respectively. T_1 is used to trigger the pulsed laser, while T_2 triggers the acquisition device. During experiments, the transducer is immersed in an ultrasonic-coupling medium (water, in this case) in a container for proper coupling of ultrasonic propagation. The TR-PAM system conforms to the biological tissue use safety limits described in the American National Standard for Safe Use of Lasers (20 mJ/cm^2).

Lateral and axial resolution were tested to verify the imaging capability of the TR-PAM system. A surgical blade was inserted into the sink and experimentally quantified by imaging the sharp-edged surgical blade, with a scanning step of ~1 μm [33]. The fitted edge-spread function (ESF) was estimated from the blade PA data along the white dashed line at the focal distance. The line-spread function (LSF) was calculated as the derivative of the ESF. The full width at half-maximum (FWHM) of the LSF, defining the highest lateral resolution, was estimated to be ~5 μm, as shown in Fig. 1(d). Fig. 1(e) shows the pulse response of the ringed focused ultrasonic transducer at the focus (black line), and the red dotted line represents the corresponding Hilbert-transformed envelope. The axial resolution can be defined as the full width at FWHM of the envelope, which is measured to be about 37.5 μm. The amplitude-frequency response of the detector is shown in Fig. 2 (f). Based on the amplitude-frequency response, it is determined that the central frequency of the transducer is about 40 MHz and the relative bandwidth (-6 dB) is ~72 MHz.

2.3. Experiment preparation

Phantom Experiments: The imaging samples with different elastic values can be represented by solidified agar solutions with varying concentrations. The samples used in the experiment were prepared using agar solutions with three concentrations: 20 g/L (w/v), 30 g/L (w/v), and 40 g/L (w/v). The specific preparation method involves mixing different weights (2 g, 3 g, and 4 g) of agar powder with distilled water, heating it in a water bath at 90 ℃, and stirring until the agar is fully dissolved. Finally, the same volume fraction of black ink (3 %) is added to all three solutions to provide optical absorption contrast as a source of chromophores.

Ex vivo Fat and Muscle Tissue Experiments: The samples were made from normal fat and muscle tissues of the same pig leg, and the fat tissue parts were stained with hematoxylin-eosin to increase the absorption of the lipid to the 532 nm laser. Due to the uneven surface of the samples after staining, this can significantly affect the resolution and signal-to-noise ratio of the TR-PAM system. Therefore, to minimize the impact of the geometric shape of the samples on PA image quality, the samples were compressed for a period using a cover glass to obtain flat tissue models. It is also important to emphasize that the additional mechanical stress is very small, which is insufficient to alter the physical and biochemical characteristics of the tissue samples. Moreover, the difference in elasticity of the tissue samples before and after the additional mechanical stress was also measured using a conventional rheometer,

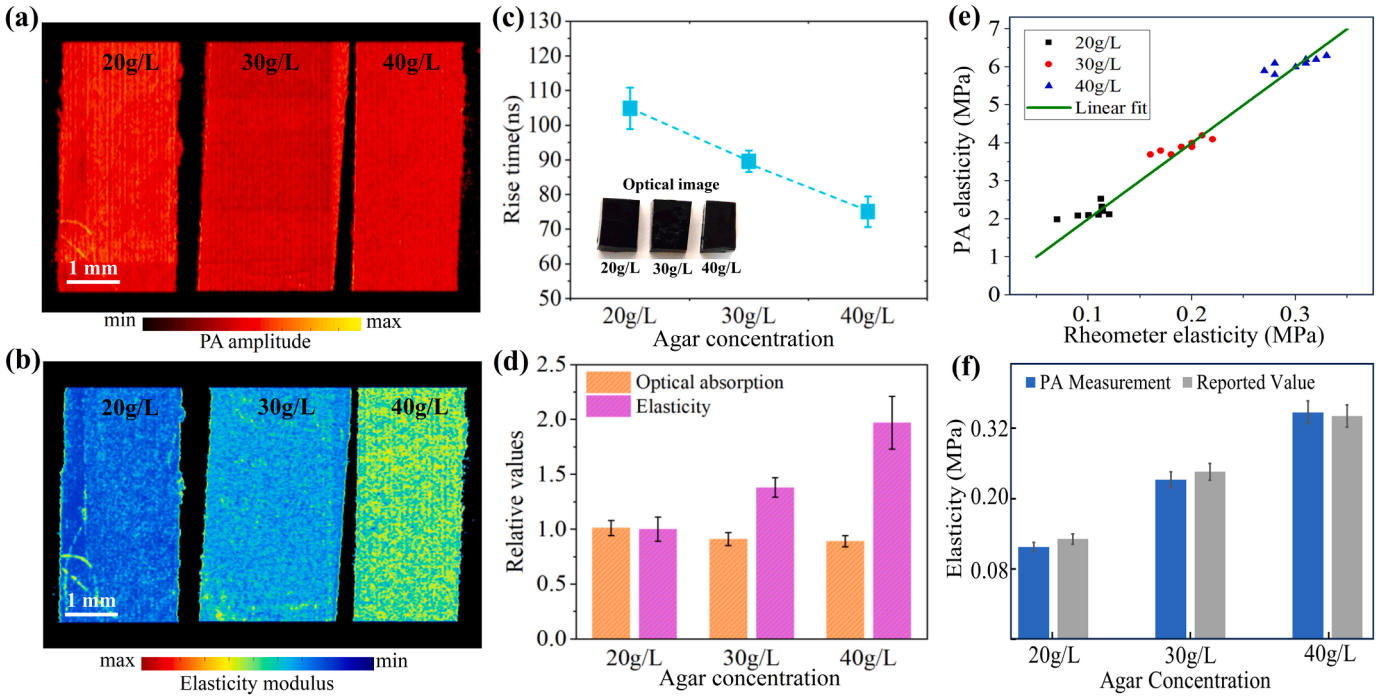

Fig. 2. Validation of the PA elasticity estimation by TR-PAM. (a) The conventional PA intensity images of agar-gelatin phantoms with different concentrations. (b) Specific PA rise time values. (c) The resulting PA elastography maps, and the optical image. (d) Optical absorption and elastic analysis. (e) Comparison of elasticity measured by the PA method and the conventional rheometer measurement results from references. (f) Comparison of the elasticity between the PA measurement results and the reported results in references.

and the elasticity remained largely unchanged.

In vivo Microvascular Experiments: Adult female mice, 6–8 weeks old (Types: ICR, DBDB, and MRL/Lpr; Quantities: 10, 5, and 5, respectively; Wukong Biotechnology Co., LTD, Jiangsu, China) were used for the in vivo experiment. Vitamin D-induced calcification in mice is currently considered to be one of the more robust models of calcification [3]. This model was prepared by injecting vitamin D3 at a single dose of 100,000 IU/kg every 2 days. The ICR mice were used to construct a model of hypervitaminosis D caused by drug overdose. The DBDB mice, prone to obesity, hyperglycemia, and hyperlipidemia, and the MRL/Lpr mice, which display symptoms similar to those of human immune complex glomerulonephritis and are often used in the study of CKD, were also injected with the same dose of vitamin D3 to accelerate the disease model development process and explore the relationship between the metabolic level of the diseased body and microvascular calcification (MC). Additionally, a group of completely healthy ICR mice (with a number of 5 ICR mice) was established as a control group to provide a baseline for comparison. These control mice received no injections and were maintained under identical conditions to ensure that any observed effects could be attributed solely to the experimental interventions, thereby enhancing the rigor and clarity of the study outcomes. The hair on the mice's ears was removed using a commercial depilatory cream (Payven Depilatory, China), and the mice were subsequently injected with sodium pentobarbital (30 mg/kg; with a supplemental dose of 10 mg/kg/h) to ensure they remained motionless before imaging.

In order to minimize the influence of factors such as blood flow and temperature on the accuracy and reliability of experimental results, the mice were subcutaneously injected with sodium pentobarbital (30 mg/kg; with a supplemental dose of 10 mg/kg/h) to induce anesthesia and were maintained with 100 % oxygen. The mice were aligned in a stereotactic frame, and their body temperature was monitored using a rectal probe, maintained with a heating pad. Warmed sterile saline was injected subcutaneously at a rate of 0.1 mL/hour to ensure hydration. Additionally, the mice received subcutaneous injections of carprofen (5 mg/kg) and dexamethasone (0.2 mg/kg) to reduce inflammation after each experiment. By controlling the above experimental conditions, the body temperature and blood flow of the mice did not vary significantly during each microvascular imaging experiment, thereby mitigating the impact of these factors on the measurement results of microvascular elasticity. Similarly, other factors, such as vessel wall thickness and vascular sclerosis, could also influence the measurement results of the elastic modulus due to changes in the microvascular physical structure or properties. While the vessel wall thickness and vascular sclerosis of the mice could change over time and with disease state, the method of self-controlled *in situ* experiments was adopted to monitor the changes in vascular elasticity at the same tissue location, ensuring that the final analysis results were not affected. Furthermore, we conducted 2–3 repeated experiments during each imaging process to reduce errors caused by these factors. For the selection of regions of interest (ROIs), we primarily considered areas with large blood vessels, as the structure of small blood vessels is not sufficiently stable, and local apoptosis may occur as diseases progress. All experimental animal procedures were carried out in accordance with a laboratory animal protocol approved by the Animal Studies Committee of Nanjing University of Science and Technology.

In vivo TR-PAM experiment: In the animal experiments involved in this study, all experimental group mice were monitored strictly at a frequency of every five days, during which attention was paid to observing indicators such as the mice's vitality and weight, with each experimental monitoring session being repeated 2–3 times. The mice were anesthetized with sodium pentobarbital injections and underwent hair removal on their ears to prevent potential impacts on imaging quality. The limbs were secured, and the mice remained still in the scanning area. The scanning parameters were as follows: the scanning range 10 mm x 10 mm, the scanning step size 5 μm, the laser wavelength 532 nm, and the laser frequency 10 kHz. To minimize the impact of the experimental environment on the results, the laboratory temperature was maintained at 25 degrees Celsius and the air humidity was kept between 40 % and 60 %.

2.4. Preparation of vascular calcification fuqiangn pathological sections

The preparation of pathological sections involves several detailed steps to ensure the tissue is ready for microscopic examination. First, the paraffin sections are dewaxed in water through a series of immersions: twice in xylene, each for 20 minutes, followed by two rounds in absolute ethanol, each lasting 5 minutes, then in 75 % ethanol for 5 minutes, with rinses in tap water and three subsequent washes in distilled water. The sections are then dried, and a barrier is created around each with a paintbrush before applying the Von Kossa stain. The slides are exposed to UV light continuously for 4 hours and then subjected to multiple washes with distilled water. Subsequently, the sections are stained with hematoxylin for 3–5 minutes, differentiated with a differentiation solution, washed in tap water, blued with a bluing reagent, and finally rinsed under running water. For eosin staining, the sections are dehydrated through a gradient of alcohol, first in 85 % ethanol for 5 minutes, followed by 95 % ethanol for another 5 minutes, then stained in eosin for a 5-minute interval. Finally, the sections undergo dehydration through three successive 5-minute periods in absolute ethanol and are cleared in two 5-minute stages in xylene before being mounted with neutral balsam. This preparation culminates in microscopic examination and image acquisition for analysis.

2.5. Statistical analysis

Unless otherwise specified, statistical analyses were performed on GraphPad Prism 6.0. Ninety measurements of the elasticity were recorded for the agar samples, fat, and muscle tissues. Four experimental groups were analyzed for elasticity evaluation of MC. Comparisons between conditions were analyzed using Student' s *t-test*. $P < 0.05$ was considered significant. Data was presented as mean ± SD.

3. Results

3.1. Phantom experiments

To demonstrate the capability of the TR-PAM imaging in bio-mechanical characterization, three tissue-mimicking agar phantoms with different agar concentrations of 20, 30, and 40 g/L were prepared and tested, as shown in Fig. 2. The conventional PAI of the three agar phantoms shown in Fig. 2(a) reflects the samples' optical absorption that corresponds to the ink concentration. The average rise times of PA signals from the three agar phantoms were then measured separately, as shown in Fig. 2(b), which demonstrated a significant difference and also indicated that the average rise time decreased with increasing agar concentration. Utilizing the measured rise time of all PA signals, the resulting TR-PAM elastic images were reconstructed in Fig. 2(c), revealing that these PA elastic images of the three agar phantoms could be clearly distinguished. As shown in Fig. 2(d), from the results of this experiment, it can be observed that there is no significant difference in their optical absorption intensity, since the three phantoms adopted the same volume fraction of black ink (3 %), but the elastic properties of the agar phantoms are positively correlated with the agar concentrations. In PA elasticity measurements, the system constant K value is defined as 1. These ρ and R values are respectively estimated to be 1.0×10^3 kg/m^3 and ~5.0 μm. Meantime, to validate the TR-PAM method's accuracy, the value of elasticity of the phantom sample was also obtained according to some reported results [34]. Utilizing the measured PA rise time, the resulting PA elastic modulus is estimated in Fig. 2(e) according to Eq. (6) reported results [34]. As expected, the elasticity increases with the agar concentration. The results reveal that there is a good correlation between rheometer and TR-PAM measurements, as shown in Fig. 2(e). The TR-PAM measurements are also in good agreement with results obtained by the equation $E_Y = 0.349\ C^{1.87}$, relating the agar concentration (C, in g/L) and Young's modulus (E_Y, in kPa) [34], as shown in Fig. 2(f). Based on these findings, it is confidently concluded that the accuracy of the TR-PAM method is reliable. Therefore, this method can be used to investigate the elastic moduli at a quantitative level and to develop micron-scale microvascular mappings of elastic properties in soft tissue.

3.2. Ex vivo tissue experiments

To further validate the capacity of the TR-PAM technique for tissue characterization, fresh *ex vivo* muscle and fat tissues from one pig leg were imaged. Fig. 3(a) shows optical absorption images of the prepared fresh *ex vivo* tissues, including muscle tissue (left panel) and fat tissue (right panel). In the conventional PA intensity image, muscle tissue appears to have a much stronger PA signal amplitude due to the stronger optical absorption compared to the fat tissue when using the 532 nm excitation laser. Utilizing the measured rise time from the two *ex vivo* tissues, the resulting TR-PAM rise time and elastic images were reconstructed, as shown in Fig. 3(b) and Fig. 3(c), respectively. The results display that the two tissue types indicate different elastic features and exhibit a clear boundary at their junction. The main reason for this phenomenon is that the mechanical properties of the two tissue types are different; typically, the muscle fiber or matrix usually has higher stiffness than the lipid, and the muscle tissue has a larger elastic modulus than the fat tissue, thus displaying clear elasticity contrast results. Meanwhile, Fig. 3(d) provides the temporal PA response of the respective fat and muscle tissues. Each curve represents an average of ten acquisitions, each repeated with the same parameters. Fig. 3(e) shows the rise time along the dotted line in Fig. 3(b). Additionally, the average optical absorption and elastic modulus of fat and muscle tissues were measured, as shown in Fig. 3(f), respectively, and the obtained elastic modulus data reveals that the muscle tissue has an increase of about 65 % over that of fat tissue. These results further confirm that the two tissues have differences in bio-mechanical properties. The significant differences observed demonstrate that the TR-PAM method can provide bio-mechanical characterization that is independent of optical absorption for the analysis and identification of tissue components.

3.3. Microvascular calcification imaging experiments

In order to demonstrate that the proposed TR-PAM technology can monitor the occurrence of MC, the hypervitaminosis D, diabetes, and CKD mice for MC models to compose the experimental samples were prepared and imaged. The number of MC monitoring of experimental mice increased with the number of days of modeling, and the experiments were conducted every 5 days, and the experimental environment remained the same each time. Each experiment was repeated three times to ensure the reliability of the results.

3.3.1. Hypervitaminosis D and MC

Excess vitamin D levels, recognized as one of the most important factors causing extensive microvascular calcification (MC), have been linked with increased cardiovascular and cerebrovascular mortality in a number of large-scale epidemiological and clinical studies [3,38,39]. However, the continuous monitoring of the MC induction process through hypervitaminosis D has yet to be fully elucidated and remains a challenge.

To verify the capability of TR-PAM technique to effectively monitor microvascular elastic parameters of hypervitaminosis D, the imaging experiments on the ICR mice model at different pathological stages (0, 5, 10, 15, and 20 days) were performed. Fig. 4(a) (first line) portrays the PA intensity images of a mouse's ear in vivo, showing that the microvascular profile could be visualized via optical absorption. The PA elastography of the mouse's ear at different stages is shown in Fig. 4(b) (second line), revealing that the microvascular profile could be displayed via elastography. Meanwhile, the average PA optical absorption and the average diameter of the main micro vessels of the mouse's ear at different stages were counted shown in Fig. 4(c) and Fig. 4(d), respectively. The results indicate that there are no significant differences

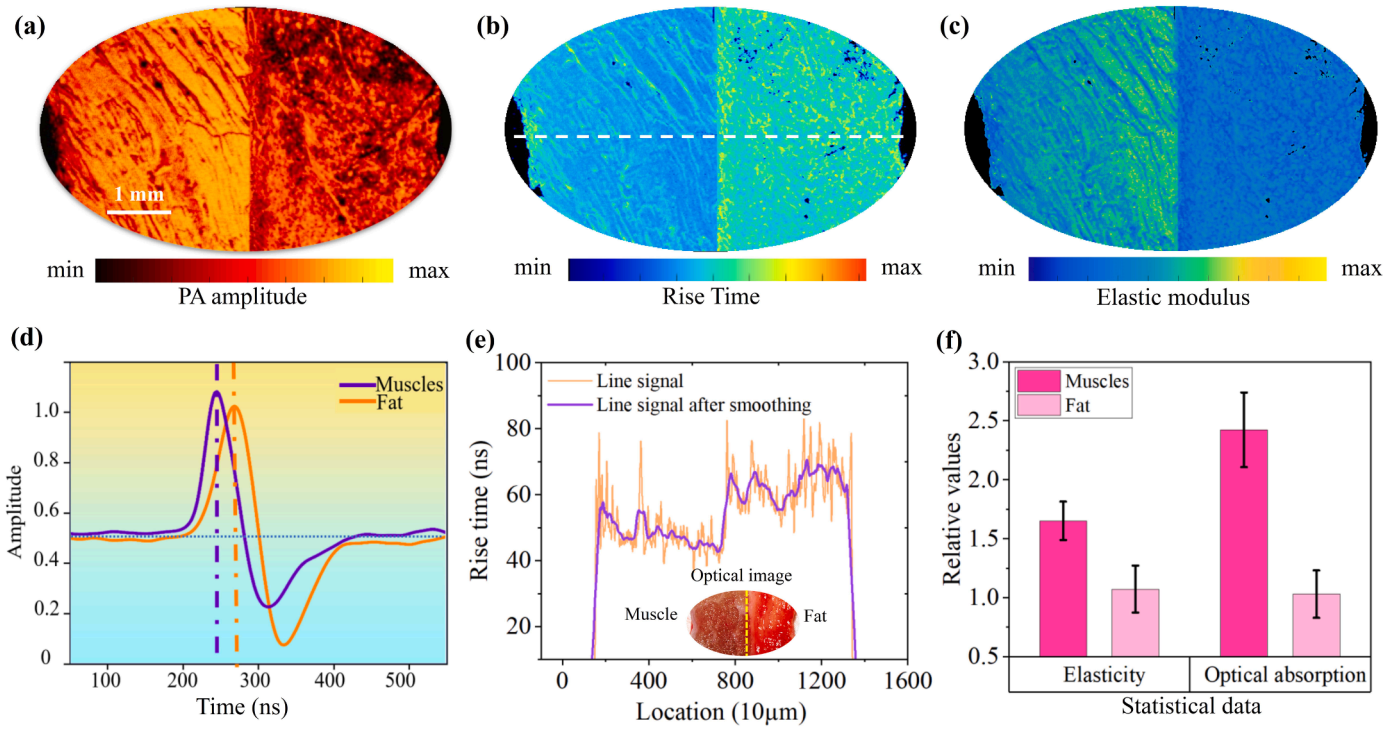

Fig. 3. Analysis and identification of different tissues by the TR-PAM. (a) The conventional PA intensity images of *ex vivo* muscle tissue (left panel), and fat tissue (right panel). (b) Maximum projection of PA rise time for the two tissues. (c) The resulting PA elastography map. (d) PA signals from muscle and fat tissues. (e) Specific PA rise time values along the dotted line in Fig. 3(b), and the optical image of muscle and fat tissues. (f) Optical absorption and elastic analysis for the two tissues.

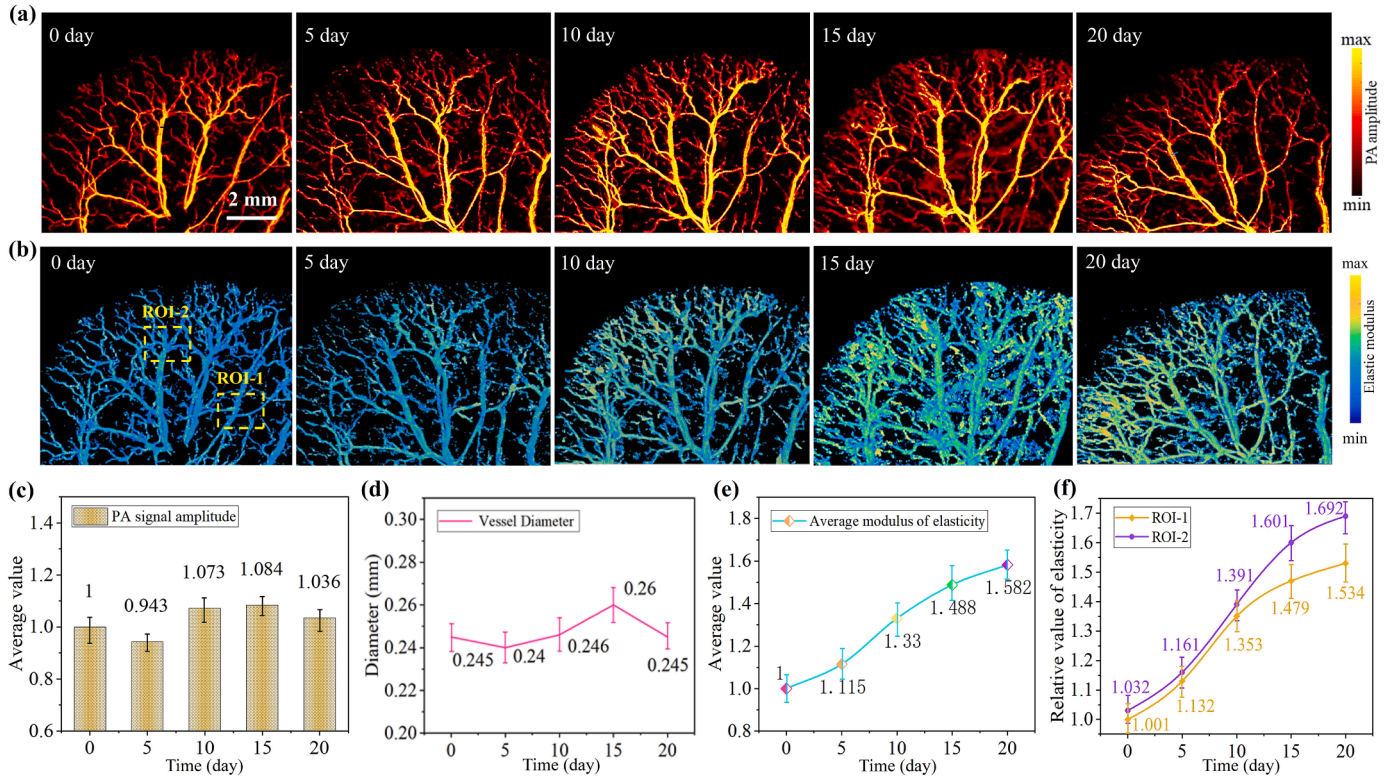

Fig. 4. Monitoring MC caused by hypervitaminosis D using the TR-PAM. (a) The conventional PA intensity images of the ICR mice model at different pathological stages (0, 5, 10, 15, and 20 days). (b) The resulting PA elastography maps. (c) Average magnitude of the optical absorption parameters. (d) Average diameter of the main micro vessels. (e) Average magnitude of the elasticity parameters. (f) the statistics of elastic modulus for two ROIs in (b).

among them, and the occurrence and progression of MC cannot be monitored by PA structural imaging of blood vessels alone ($P > 0.05$). Fig. 4(e) indicates that the statistical value of the average microvascular elastic modulus increases over the days. Compared with the result of the first observation (0 day), the average value of the elastic modulus on the 20th day has increased by about 58 %, aligning with the expected results of the experiment ($P < 0.05$). Fig. 4(f) presents the elastic statistics of different ROIs. By utilizing the elastic data of ROIs (1, and 2) in the PA elastic image of the first observation (0 day) as the reference value, it can be seen that the elastic modulus of both ROIs increases with the molding days ($P < 0.05$), but the amount of growth for two regions is different. According to the previously mentioned formula (7), there is a positive correlation between the calcification extent and the elasticity of blood vessels. Therefore, these results also imply that differences in the microvascular elasticity at different sites can represent differences in the degree of MC, enabling clear differentiation between various degrees of MC and calcification locations.

So to wrap up here, the study produced a variant of this hypervitaminosis D model in which ICR mice initially treated with a dose (100,000 IU/kg/2 days) for 20 consecutive days, developed diffuse and widespread MC outcomes of soft tissue that had been monitored in a time-dependent manner in mice by the proposed TR-PAM technique.

3.3.2. *Diabetes and MC*

Microangiopathy has long been recognized as a major complication of diabetes, manifested by dermopathy, retinopathy, neuropathy, and nephropathy. Indeed, previous studies have linked these symptoms to calcification of diseased capillaries, arterioles, and venules [6]. In the skin, superficial soft tissue ischemia resulting from microvascular calcification (MC) particularly affects the lower extremities and accelerates the development of diabetic foot ulcers [40,41]. Many functional and structural abnormalities of the subcutaneous microvessels have been observed in diabetes, highlighting the complexity of the pathological processes. However, monitoring the development of MC at different stages of the disease has yet to be fully investigated and continues to pose technical difficulties.

A significant feature of diabetic microangiopathy is the decrease in microvascular elasticity caused by MC, which has been related to poor glycemic control and to the metabolic abnormalities of diabetes [6]. To further demonstrate that TR-PAM can facilitate observation of changes in the MC, one representative experiment was conducted in diabetic mice model with different pathological states. In addition, to accelerate the development of MC, and simulate metabolic abnormalities caused by improper regulation of vitamin overdose in this animal model, one DBDB mouse was also injected with the same dose of vitamin D3 in the ICR mice. Fig. 5(a) and Fig. 5(b) are the PA intensity images (first line) and PA elastic images (second line) of one *in vivo* DBDB mouse's ear at 5 time points (after 0, 5, 10, 15, and 20 days), respectively. Fig. 5(c) and Fig. 5(d) show that the average PA intensity and the average diameter of the main micro vessels of the mouse's ear at different time points were counted, respectively. Similarly, the occurrence and progression of MC in the DBDB mouse model cannot be monitored by PA absorption imaging of blood vessels alone ($P > 0.05$). Fig. 5(e) shows the statistics of the average vascular elastic modulus. With the progression of days, the average vascular elastic modulus of the 5th, 10th, 15th, and 20th days increased by about 21 %, 42 %, 52 %, and 62 % respectively, compared with the result of the first experiment (0 day), which represented a change of MC in the upward trend ($P < 0.05$). Fig. 5(f) shows the elastic statistical results of the three ROIs. Utilizing the elastic data detected for the first time point (0 day) in ROIs (1, 2, and 3) as the reference value, the vascular elastic values of the three ROIs demonstrated an upward trend ($P < 0.05$). Compared with the elastic value measured at the first time point (0 day), the statistical average increase of the three ROIs was about 120 %, which was larger than the increase of the elastic value in Fig. 5(e). These results suggest that the TR-PAM technology supports microvascular level mappings of elastic properties *in vivo*, and can

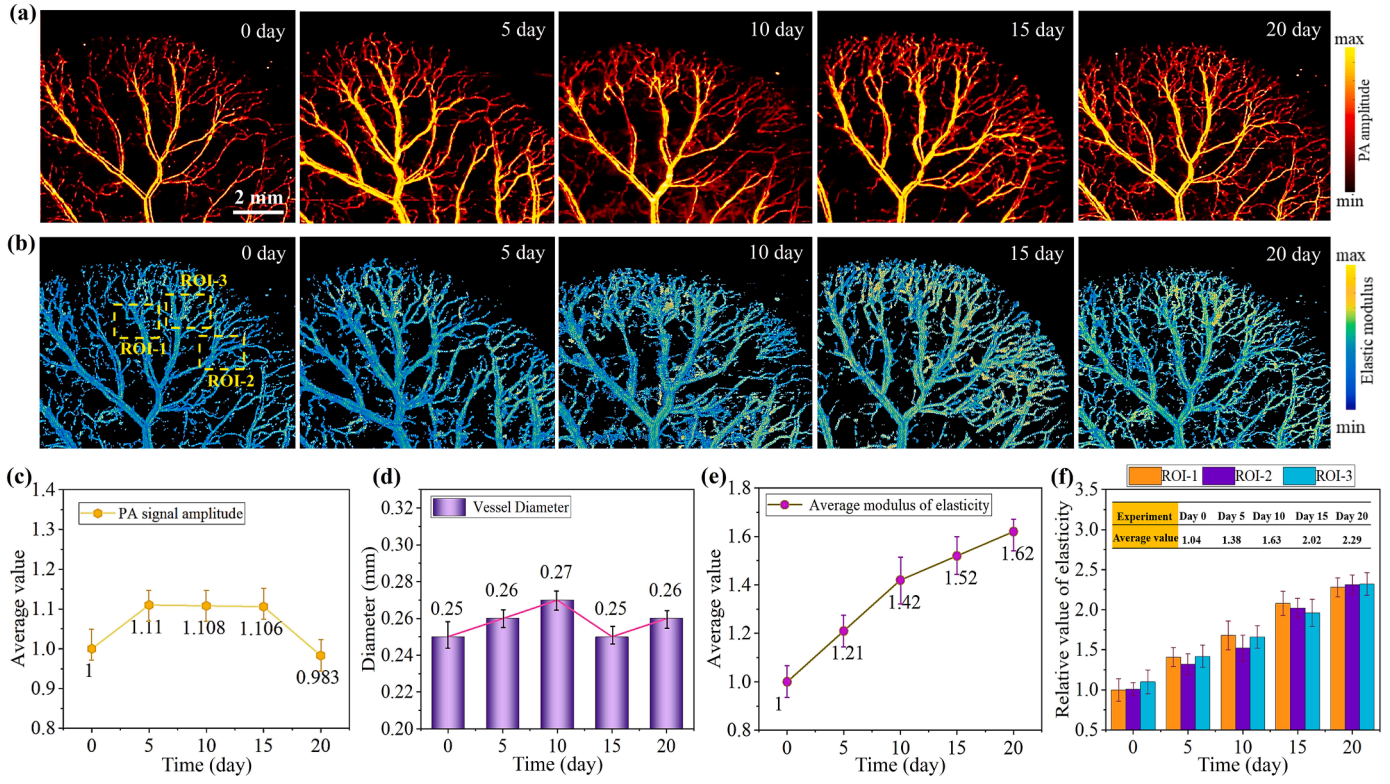

Fig. 5. Monitoring MC caused by diabetes using the TR-PAM. (a) The conventional PA intensity images of one *in vivo* DBDB mouse's ear at 5 time points (after 0, 5, 10, 15, and 20 days). (b) The resulting PA elastography maps. (c) Average magnitude of the optical absorption parameters. (d) Average diameter of the main micro vessels. (e) Average magnitude of the elasticity parameters. (f) the statistics of elastic modulus for three ROIs in (b).

enable continuous monitoring of the elastic parameters for development process of MC related to diabetes as per the aforementioned formula (7). In addition, it can be also seen that small blood vessels and terminal vessels are more prone to calcification, as indicated by the results in Fig. 5(b), so the method can be also used to distinguish the degree and location of MC.

Therefore, the potentiation between structural and functional abnormalities, especially in the presence of MC in the superficial soft tissue (which is itself closely related to microvascular impairment), may explain why diabetic ulcers develop on the foot from the results in Fig. 5. Also, the difference in terminal micro vessels and microvascular diameter among foots might contribute to the risk of diabetic foot ulcers.

3.3.3. *CKD and MC*

As microvascular calcification (MC) frequently occurs with chronic kidney disease (CKD), initial thoughts on its risk factors were centered on outcomes from metabolic disorders. Clinically, patients with genetic defects, drug abuse, or metabolic disorders frequently develop MC, which is deemed to augment susceptibility to CKD-related events [3,4]. Early interventions for MC are predicated on correcting general metabolic disorders that compromise CKD health [3,6]. The primary limitation that clinicians currently face in considering these traditional risk factors for CKD treatment is that they fail to continuously monitor a large number of microvascular characteristics, particularly those which manifest in differences in MC.

To further demonstrate that TR-PAM can facilitate monitoring of characteristics in the MC for CKD disease, another representative experiment was performed in CKD mice model with different pathological states. Similarly, to accelerate the development of MC, and simulate metabolic abnormalities caused by improper regulation of vitamin overdose in this animal model, the MRL/Lpr mouse was also injected with the same dose of vitamin D3 as given to the ICR mice. Fig. 6(a) and Fig. 6(b) are the PA intensity images (first line) and PA elastic images (second line) of one *in vivo* MRL/Lpr mouse's ear at 4 time points (after 0, 5, 10, and 15 days), respectively. Fig. 6(c) displays that the average PA intensity of the micro vessels in the mouse's ear at different time points were counted. The statistical result suggests that there is no significant change ($P > 0.05$) in this PA intensity images in Fig. 6(a). Moreover, Fig. 6(d) shows the result of average values of vascular elastic modulus. With the progression of modeling days, the average value of the vascular elastic modulus on the 5th, 10th and 15th days increased by about 30 %, 40 % and 60 % respectively, compared with the result of the first experiment (0 day), which also indicated an upward trend ($P < 0.05$). Fig. 6(e) reveals the statistical elastic results of the two ROIs (1, and 2). With the elastic tested for the first time (0 day) in the ROIs as the reference value, the vascular elastic value of the ROIs demonstrated an upward trend, and the total increase of the average elastic modulus of the two ROIs was about 72 %, which was similar to the previous experimental results and in line with the experimental expectations ($P < 0.05$). These results clearly demonstrate that PA elastic imaging can differentiate between detecting different degrees of vascular calcification and is a viable and alternative tool to existing clinical diagnostic techniques.

Therefore, a complex MC development process involving physiochemical changes to metabolic abnormality has been demonstrated in this CKD model by the proposed TR-PAM method. In particular, MC resulting from modifications to vitamin D homeostasis of CKD disease has been simulated and elucidated. The PA elastic results obtained by

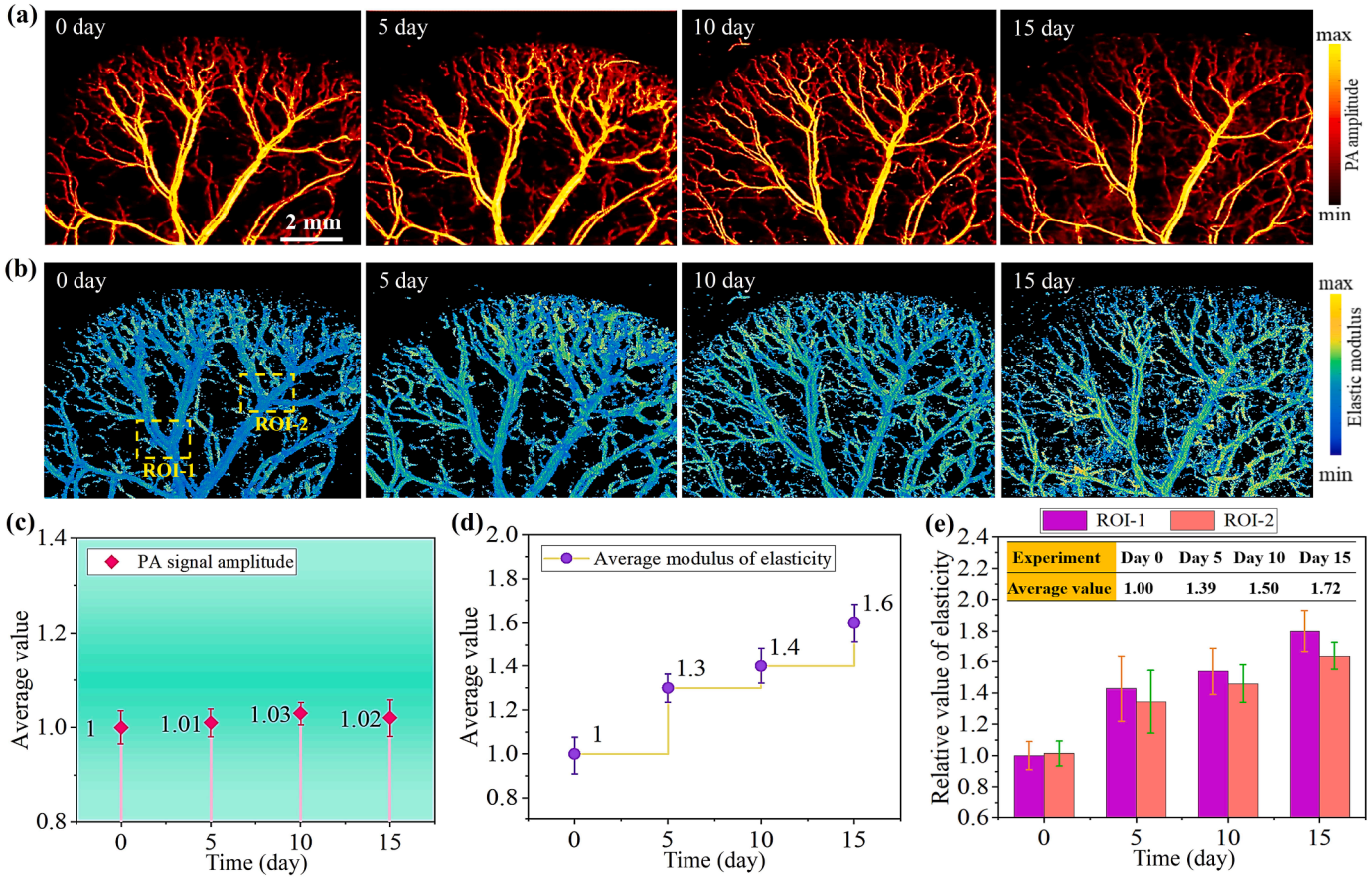

Fig. 6. Monitoring MC caused by CKD using the TR-PAM. (a) The conventional PA intensity images of one *in vivo* MRL/Lpr mouse's ear at 4 time points (after 0, 5, 10, and 15 days). (b) The resulting PA elastography maps. (c) Average magnitude of the optical absorption parameters. (d) Average magnitude of the elasticity parameters. (e) the statistics of elastic modulus for two ROIs in (b).

TR-PAM can distinctly display the bio-mechanical differences of micro vessels in the CKD mice model at different pathological states. Thus, the significant differences observed demonstrate that the TR-PAM technology can provide information on mechanical properties that is independent of optical absorption for identifying MC in CKD.

3.3.4. Control tests

After conducting experiments on specific animal models, continuous monitoring was also performed on the same regions in healthy, disease-free mice to serve as references for subsequent observations in animal model experiments. Fig. 7(a) displays the PA intensity images of one *in vivo* mouse's ear captured in vivo over various periods (0, 5, 10, 15, and 20 days), demonstrating that the microvascular profile is visible through optical absorption. The PA elastography of the mouse's ear at different stages are shown in Fig. 7(b). Meanwhile, the average PA optical absorption and the average diameter of the main micro vessels of the mouse's ear at different stages were counted shown in Fig. 7(c) and Fig. 7(d), respectively. The results indicate that there are no significant differences among them (P >0.05). Fig. 7(e) illustrates that the statistical value of average microvascular elastic modulus, which basically stayed flat with the molding days ($P > 0.05$). Fig. 7(f) shows the elastic statistics of different ROIs. Utilizing the elastic data of ROIs (1, and 2) in the PA elastic image of the first observation (0 day) as the reference value, it can be seen that the elastic modulus of both ROIs doesn't change much with the molding days ($P > 0.05$). Thus, these results also affirm the reliability and precision of the TR-PAM technique, facilitating the clear differentiation of various degrees of MC.

The data presented in Fig. 8(a)-(g) provide a comprehensive analysis of microvascular calcification in healthy mice compared to those affected by elevated vitamin D levels (Hyp. D), diabetes, and CKD. The results from these four pairs of optical images show that it is very difficult to observe the differences in blood vessels solely from optical images, and almost no pathological changes can be seen ($P > 0.05$). In healthy mice, there were no evident signs of calcification on day 20 compared to day 0, as illustrated in Fig. 8(a). Conversely, mice with elevated vitamin D levels showed distinct structural disruptions and calcification on day 20 when compared to day 0, particularly in regions highlighted by blue arrows in Fig. 8(b). Similarly, diabetic mice exhibited subtle yet discernible structural changes and early signs of calcification on day 20 compared to day 0, as depicted in Fig. 8(c). The most pronounced alterations were observed in the CKD models, where significant microvascular calcification was evident on day 20 compared to day 0, as shown in Fig. 8(d). The quantitative segment of the study, detailed in Fig. 8(e)-(g), further substantiates these observations. An analysis of average optical density across the slices indicates a uniform baseline at day 0 across all groups. However, a marked increase in optical density was noted in the disease models on day 20 compared to day 0, signifying a progressive calcification process ($P < 0.05$). The proportion of calcification also increased under all disease conditions on day 20 compared to day 0 ($P < 0.05$). The calcification density graph corroborates these findings, with all disease models exhibiting a substantial increase in calcification density over the monitoring period, particularly noticeable when comparing day 20 to day 0, as shown in Fig. 8(g), whereas the increments in healthy mice were minimal ($P > 0.05$).

Overall, these results demonstrate that mice under pathological conditions such as high vitamin D, diabetes, and CKD exhibit a faster and more significant rate of microvascular calcification compared to healthy mice. Each experimental condition was replicated three times to ensure the reliability and reproducibility of the findings. The TR-PAM measurements consistently demonstrated the progressive development of MC, with minor deviations observed across replicates. These deviations were largely attributed to biological variability among individual mice and slight differences in injection volume. The consistency of MC outcomes and the quantifiable nature of the progression observed affirm the robustness and precision of the TR-PAM technique in capturing dynamic pathological changes in this model. This further verifies the accuracy of the calcification phenomena measured by the TR-PAM system. These findings provide a strong experimental basis for further studies into the long-term effects of these chronic diseases on microvascular structure

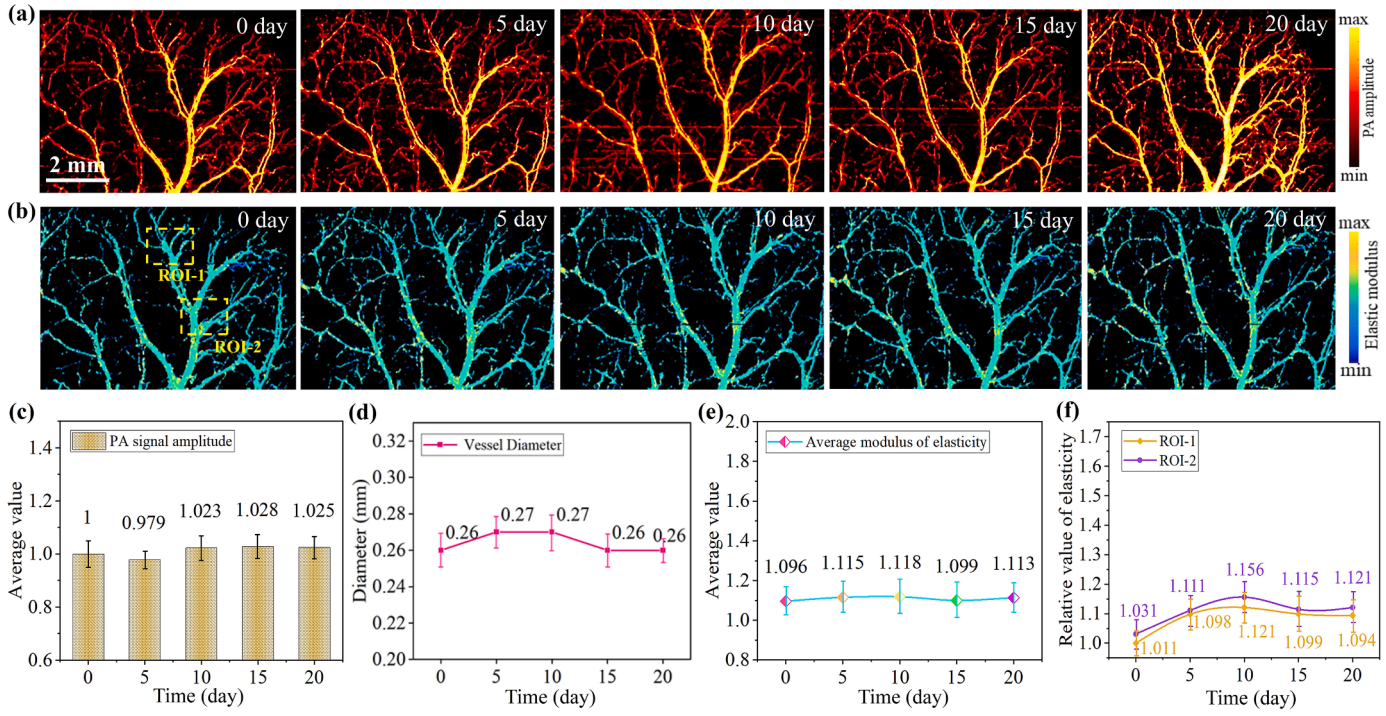

Fig. 7. Monitoring healthy group using the TR-PAM. (a) The conventional PA intensity images of the ICR mice model at different pathological stages (0, 5, 10, 15, and 20 days). (b) The resulting PA elastography maps. (c) Average magnitude of the optical absorption parameters. (d) Average diameter of the main micro vessels. (e) Average magnitude of the elasticity parameters. (f) the statistics of elastic modulus for two ROIs in (b).

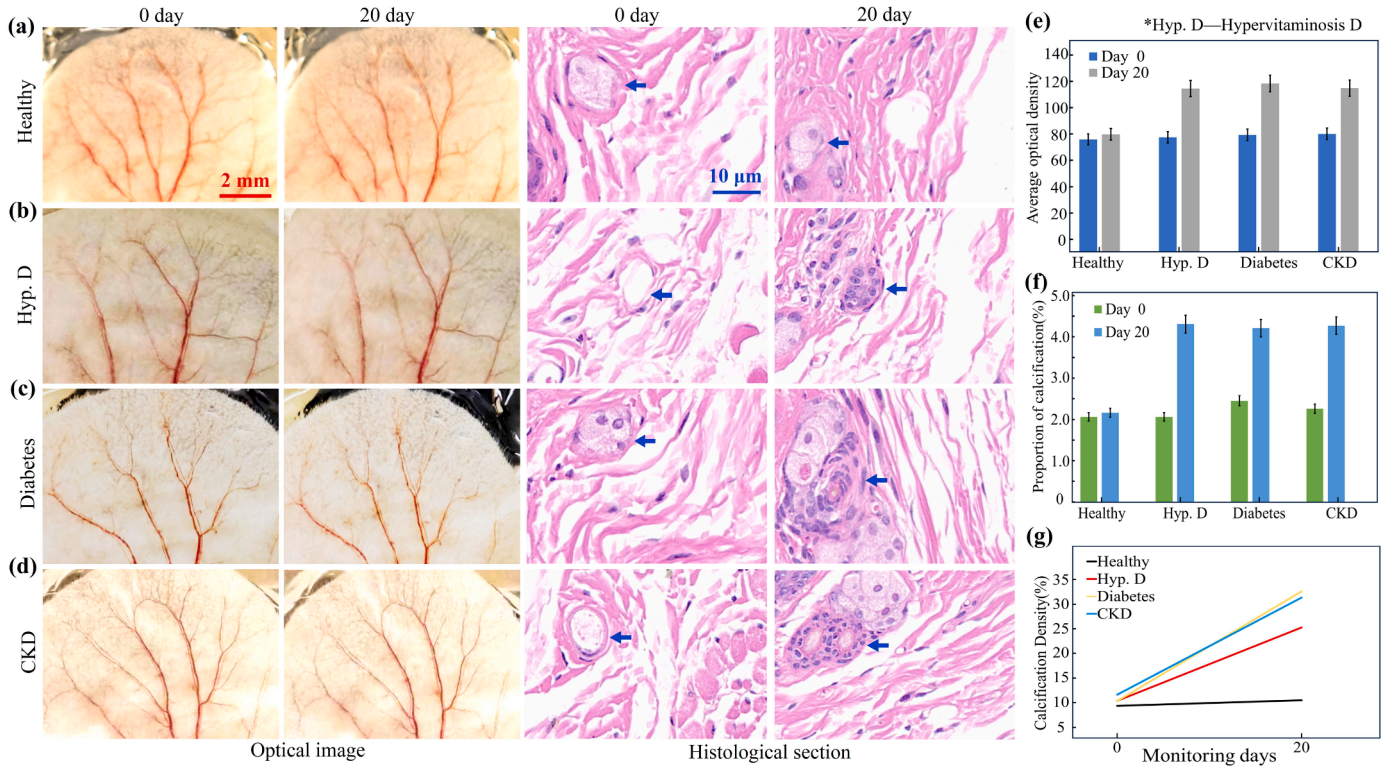

Fig. 8. Von Kossa histopathological validation. (a)-(d) Comparison of 0 and 20 day's optical images and histopathological slice images for the four experimental groups. The blue arrows point to the corresponding microvascular. (e) Average optical density from histopathological slices. (f) Proportion of calcification from histopathological slices. (g) Calcification density in histopathological photographs on 0 and 20 day across four experimental groups.

and function.

4. Discussion and conclusion

In this study, a TR-PAM method based on the detection of laser-induced transient stress has been proposed, which can be used to extract the elastic properties for monitoring and evaluation of MC in soft tissue. Different from conventional PAI, TR-PAM utilizes the rise time characteristic of PA response to extract unique microvascular elastic information. The TR-PAM method calculates elasticity moduli by analyzing the temporal characteristics of the PA response without tracking wave propagation in complex, heterogeneous soft tissues. This approach leverages the temporal response characteristics at the excitation point source of the microvascular, enabling retrieval of in situ mechanical properties at a microscopic scale. Importantly, the method does not require prior knowledge of the direction of wave propagation, as PA waves are omnidirectional elastic waves generated by the volumetric expansion of microvascular tissues. Furthermore, the reliance on vascular elastic changes, rather than the composition of blood, ensures that the method remains robust under varying physiological conditions. As the extended capability of PAI, the TR-PAM technology opens new avenues for PA elasticity imaging by providing micron-scale and tissue-level mappings of MC.

However, there are still some limitations in the TR-PAM method. (i) The influences of target shape and electronic noise on the detection of rise time of PA signal lowers the detection accuracy of the elastic detection of biological tissue, thus affecting the monitoring and evaluation of MC extent in clinical application. (ii) Limited by the size and scanning speed of the 2D motor platform, the current TR-PAM system cannot achieve fast real-time imaging, and integrated wearable and continuate monitoring device. (iii) PA signal crosstalk in one-dimensional A-line direction (Z direction) for the extraction of rise time, the TR-PAM is difficult to provide 3D information about the mechanical properties of microelastomers in deep tissue. To enhance the potential for clinical translation, the following approaches may be considered. Firstly, in terms of component design and fabrication, the size, shape, and fabrication metrics of the system are optimized to improve the sensitivity and specificity of the TR-PAM, achieving miniaturization of the device with integration of high stability and accuracy. Secondly, future advancements require the development of high performance wearable materials with non-toxicity and high biocompatibility, particularly for the contact surface with human skin. Thirdly, advanced algorithms may be employed to achieve superior imaging resolution and to assist with artificial intelligence (AI)-driven MC monitoring capabilities. Imaging algorithms can mitigate signal crosstalk and enhance the resolution of PA imaging, particularly for deeper tissues. Additionally, it is imperative to establish and develop the monitoring standards and regulations, ensuring data privacy and securing data transmissions to prevent unauthorized access to sensitive information, thus enhancing the security of TR-PAM devices in clinical environments.

In conclusion, this work focuses on developing a TR-PAM elastography method to investigate the elastic moduli at a micron-scale tissue level in *vivo*, and can enable preliminary monitoring of the elastic parameters for development process of the MC related animal models of diseases. We first proposed the feasibility of applying this method to MC repeated monitoring and conducted preliminary experimental verification. However, it was not currently possible to achieve real-time imaging in this work due to the hardware and performance limitations of the system. Addressing real-time imaging and correcting noise and shape-related inaccuracies are just some of the challenges that we aim to resolve in future steps, which were not covered in this work. Although the TR-PAM method is not yet mature and has a long way to go in research studies, with the efforts of researchers, we firmly believe that it can achieve wearable real-time MC monitoring in near future and provide the capacity to prevent and control the outbreak of major diseases.

Additionally, the elasticity imaging depth and the "signal crosstalk in A-lines" are affected by the ultrasonic transducer. The higher the center frequency and the wider the bandwidth of the ultrasonic transducer, the less signal crosstalk in A-lines will occur, but it also reduces the imaging depth of the system. In this work, the transducer owns a central frequency (-6dB) of 40 MHz, and a relative bandwidth (-6dB) of ~72 MHz, so that it can be used to detect PA signals with ~ 25 ns temporal resolution (axial resolution: ~ 37.5 μm). That is, the "signal crosstalk in A-lines" is likely negligible when the axial distance between the two samples is less than 37.5 μm, and the elasticity imaging depth in the skin can reach a depth of 3–7 mm without considering the propagation of photon. Therefore, determining how to obtain the maximum imaging depth while avoiding signal crosstalk remains a very critical task, depending on the characteristics of the imaging targets.

The technique was experimentally verified on agar phantoms and *ex vivo* fat and muscle tissues, corresponded well with the expected results. TR-PAM can obtain micron-scale and tissue-level elastic images of living biological structures. Animal MC models of hypervitaminosis D, diabetes, and CKD were tested to demonstrate TR-PAM as potential elastic technique for long-term and continuous monitoring MC induced the excess exogenous vitamin D or metabolic diseases. Therefore, the presented PA elastography method for MC monitoring in soft tissue has the potential to improve the diagnostic accuracy and facilitate early intervention of diseases, which can ultimately result in better outcomes.

CRediT authorship contribution statement

Yinshi Yu: Writing – review & editing, Writing – original draft, Visualization, Data curation. **Haigang Ma:** Writing – review & editing, Writing – original draft, Resources, Funding acquisition, Data curation, Conceptualization. **Ying Gu:** Resources. **Haixia Qiu:** Resources, Investigation, Funding acquisition. **Hongjun Wu:** Resources, Formal analysis, Data curation. **Yahui Zhu:** Writing – review & editing, Writing – original draft, Visualization, Data curation. **Chao Zuo:** Resources, Funding acquisition, Conceptualization. **Qian Chen:** Resources, Funding acquisition.

Declaration of Competing Interest

The authors declare that there are no conflicts of interest.

Acknowledgements

This work was supported by National Natural Science Foundation of China (62227818, 12204239, 62275121, 62227823, 62405137), Youth Foundation of Jiangsu Province (BK20220946), Fundamental Research Funds for the Central Universities (30923011024), and Open Research Fund of Jiangsu Key Laboratory of Spectral Imaging & Intelligent Sense (JSGP202201). We appreciate Prof. Ting Feng (Fudan University) for her assistance in this work.

Data Availability

Data will be made available on request.

References

[1] A. Amaya-Garrido, M. Brunet, B. Buffin-Meyer, A. Piedrafita, L. Grzesiak, E. Agbegbo, J. Klein, Calprotectin is a contributor to and potential therapeutic target for vascular calcification in chronic kidney disease, Sci. Transl. Med. 15 (712) (2023) eabn5939. ⟨https://www.science.org/doi/10.1126/scitranslmed.abn5939⟩.

[2] S.E.P. New, E. Aikawa, Molecular imaging insights into early inflammatory stages of arterial and aortic valve calcification, Circ. Res. 108 (11) (2011) 1381–1391, https://doi.org/10.1161/CIRCRESAHA.110.23414.

[3] J. Wang, J.J. Zhou, G.R. Robertson, V.W. Lee, Vitamin D in vascular calcification: a double-edged sword? Nutrients 10 (5) (2018) 652, https://doi.org/10.3390/nu10050652.

[4] U.A.A.S.El Din, M.M. Salem, D.O. Abdulazim, Vascular calcification: when should we interfere in chronic kidney disease patients and how? World J. Nephrol. 5 (5) (2016) 398–417, https://doi.org/10.5527/wjn.v5.i5.398.

[5] G.A. Rosito, J.M. Massaro, U. Hoffmann, F.L. Ruberg, A.A. Mahabadi, R.S. Vasan, C.J. O'Donnell, C.S. Fox, Pericardial fat, visceral abdominal fat, cardiovascular disease risk factors, and vascular calcification in a community-based sample: the framingham heart study, Circulation 117 (2008) 605–613, https://doi.org/10.1161/CIRCULATIONAHA.107.743062.

[6] J.-L. Cracowski, M. Roustit, "Human Skin Microcirculation," *Comprehensive*, Physiology 10 (2020) 1105–1154.

[7] N. Torremade, M. Bozic, S. Panizo, S. Barrio-Vazquez, J.L. Fernandez-Martin, M. Encinas, D. Goltzman, M.V. Arcidiacono, E. Fernandez, J.M. Valdivielso, Vascular calcification induced by chronic kidney disease is mediated by an increase of 1alpha-hydroxylase expression in vascular smooth muscle cells, J. Bone Miner. Res. 31 (2016) 1865–1876, https://doi.org/10.1002/jbmr.2852.

[8] S. Kayaniyil, R. Vieth, R. Retnakaran, J.A. Knight, Y. Qi, H.C. Gerstein, A.J. Hanley, Association of vitamin D with insulin resistance and β-cell dysfunction in subjects at risk for type 2 diabetes, Diabetes Care 33 (2010) 1379–1381, https://doi.org/10.2337/dc09-2321.

[9] A.S. Nurrachman, A. Azhari, L. Epsilawati, F. Pramanik, Temporal pattern of micro-CT angiography vascular parameters and VEGF mRNA expression in fracture healing: a radiograph and molecular comparison, Eur. J. Dent. 17 (02) (2023) 283–295, https://doi.org/10.1055/s-0042-1757466.

[10] E.R. Smith, T.D. Hewitson, S.G. Holt, Diagnostic tests for vascular calcification, Adv. Chronic Kidney Dis. 26 (6) (2019) 445–463, https://doi.org/10.1053/j.ackd.2019.07.001.

[11] G. Van den Bergh, B. Opdebeeck, C. Neutel, P.J. Guns, G. De Meyer, P. d'Haese, A. Verhulst, Towards a better understanding of arterial calcification disease progression in CKD: investigation of early pathological alterations, Nephrol. Dial. Transplant. 38 (5) (2023) 1127–1138, https://doi.org/10.1093/ndt/gfac301.

[12] A.L. Durham, M.Y. Speer, M. Scatena, C.M. Giachelli, C.M. Shanahan, Role of smooth muscle cells in vascular calcification: implications in atherosclerosis and arterial stiffness, Cardiovasc. Res. 114 (4) (2018) 590–600, https://doi.org/10.1093/cvr/cvy010.

[13] J.T. Pruijssen, F.H. Schreuder, J. Wilbers, J.H. Kaanders, C.L. de Korte, H. Hansen, Performance evaluation of commercial and non-commercial shear wave elastography implementations for vascular applications, Ultrasonics 140 (2024) 107312, https://doi.org/10.1016/j.ultras.2024.107312.

[14] I. Sack, Magnetic resonance elastography from fundamental soft-tissue mechanics to diagnostic imaging, Nat. Rev. Phys. 5 (1) (2023) 25–42. ⟨https://www.nature.com/articles/s42254-022-00543-2⟩.

[15] Y. Han, L. Zhang, L. Kong, G. Wang, Z. Ye, Investigating the relationship between residual stress and micromechanical properties of blood vessels using atomic force microscopy, Microsc. Res. Tech. 87 (8) (2024) 1678–1692, https://doi.org/10.1002/jemt.24552.

[16] J. Chen, H. Wang, H. Zhang, Q. Guo, X. Lin, H. Liu, C. Sun, Feasibility of nondestructive measurement of 3D vascular intramural strains by optical coherence elastography based on distortion correction and digital volume correlation, Exp. Mech. 63 (2023) 915–923, https://doi.org/10.1007/s11340-023-00960-z.

[17] M.S. Singh, A. Thomas, Photoacoustic elastography imaging: a review, J. Biomed. Opt. 24 (4) (2019) 040902, https://doi.org/10.1117/1.JBO.24.4.040902.

[18] A.B.E. Attia, G. Balasundaram, M. Moothanchery, U.S. Dinish, R. Bi, V. Ntziachristos, M. Olivo, A review of clinical photoacoustic imaging: current and future trends, Photoacoustics 16 (2019) 100144, https://doi.org/10.1016/j.pacs.2019.100144.

[19] Y. Yu, T. Feng, H. Qiu, Y. Gu, Q. Chen, C. Zuo, H. Ma, Simultaneous photoacoustic and ultrasound imaging: A review, Ultrasonics (2024) 107277, https://doi.org/10.1016/j.ultras.2024.107277.

[20] L. Lin, L.V. Wang, The emerging role of photoacoustic imaging in clinical oncology, Nat. Rev. Clin. Oncol. 19 (2022) 365–384. ⟨https://www.nature.com/articles/s41571-022-00615-3⟩.

[21] W. Choi, B. Park, S. Choi, D. Oh, J. Kim, C. Kim, Recent advances in contrast-enhanced photoacoustic imaging: overcoming the physical and practical challenges, Chem. Rev. 123 (11) (2023) 7379–7419, https://doi.org/10.1021/acs.chemrev.2c00627.

[22] C. Yang, H. Lan, F. Gao, F. Gao, Review of deep learning for photoacoustic imaging, Photoacoustics 21 (2021) 100215, https://doi.org/10.1016/j.pacs.2020.100215.

[23] Y. Gao, T. Feng, H. Qiu, Y. Gu, Q. Chen, C. Zuo, H. Ma, 4D spectral-spatial computational photoacoustic dermoscopy, Photoacoustics 34 (2023) 100572, https://doi.org/10.1016/j.pacs.2023.100572.

[24] H. Ma, Z. Cheng, Z. Wang, H. Qiu, T. Shen, D. Xing, Y. Gu, S. Yang, Quantitative and anatomical imaging of dermal angiopathy by noninvasive photoacoustic microscopic biopsy, Biomed. Opt. Express 12 (10) (2021) 6300–6315, https://doi.org/10.1364/BOE.439625.

[25] Y. Liu, Z. Zou, S. Wang, C. Tao, Z. Hu, X. Liu, Wavelet-based photoacoustic viscoelastographic microscopy using photoacoustic damped oscillation effect, Appl. Phys. Lett. 124 (13) (2024) 133701, https://doi.org/10.1063/5.0198270.

[26] P. Hai, Y. Zhou, L. Gong, L.V. Wang, Quantitative photoacoustic elastography in humans, J. Biomed. Opt. 21 (2016) 066011, https://doi.org/10.1117/1.JBO.21.6.066011.

[27] P. Hai, Y. Zhou, L. Gong, L.V. Wang, Photoacoustic elastography, Opt. Lett. 41 (2016) 725, https://doi.org/10.1364/OL.41.000725.

[28] Y. Liu, C. Tao, X. Liu, Photoacoustic multispectral elastography based on the photoacoustic oscillation effect for microelastomers in deep tissue, Phys. Rev. Appl. 20 (2) (2023) 024035, https://doi.org/10.1103/PhysRevApplied.20.024035.

[29] S. Du, Z. Chen, D. Xing, Spectral interferometric depth-resolved photoacoustic viscoelasticity imaging, Opt. Lett. 46 (7) (2021) 1724–1727, https://doi.org/10.1364/OL.415368.
[30] D. Yang, Z. Chen, D. Xing, A novel needle probe for deeper photoacoustic viscoelasticity measurement, Chin. Opt. Lett. 20 (8) (2022) 081701. ⟨https://opg.optica.org/col/abstract.cfm?uri=col-20-8-081701⟩.
[31] Q. Wang, Y. Shi, F. Yang, S. Yang, Quantitative photoacoustic elasticity and viscosity imaging for cirrhosis detection, Appl. Phys. Lett. 112 (2018) 211902, https://doi.org/10.1063/1.5021675.
[32] P. Wang, Z. Chen, D. Xing, Multi-parameter characterization of atherosclerotic plaques based on optical coherence tomography, photoacoustic and viscoelasticity imaging, Opt. Express 28 (2020) 13761, https://doi.org/10.1364/OE.390874.
[33] F. Yang, W. Ding, X. Fu, W. Chen, J. Tang, Photoacoustic elasto-viscography and optical coherence microscopy for multi-parametric ex *vivo* brain imaging, Biomed. Opt. Express 14 (11) (2023) 5615–5628, https://doi.org/10.1364/BOE.503847.
[34] F. Yang, Z. Chen, P. Wang, Y. Shi, Phase-domain photoacoustic mechanical imaging for quantitative elastography and viscography, IEEE Trans. Biomed. Eng. 71 (8) (2024) 2330–2340, https://doi.org/10.1109/TBME.2024.3368150.
[35] F. Gao, X. Feng, Y. Zheng, C.D. Ohl, Photoacoustic resonance spectroscopy for biological tissue characterization[J], 067006-067006, J. Biomed. Opt. 19 (6) (2014), https://doi.org/10.1117/1.jbo.19.6.067006.
[36] R. Zhang, F. Gao, X. Feng, S. Liu, R. Ding, Y. Zheng, Photoacoustic resonance imaging, IEEE J. Sel. Top. Quantum Electron. 25 (1) (2018) 1–7, https://doi.org/10.1109/JSTQE.2018.2827660.
[37] C. Liu, J. Chen, Y. Zhang, J. Zhu, L. Wang, Five-wavelength optical-resolution photoacoustic microscopy of blood and lymphatic vessels, 016002-016002, Adv. Photonics 3 (1) (2021), https://doi.org/10.1117/1.AP.3.1.016002.
[38] Y.H. Kang, J.S. Jin, D.W. Yi, S.M. Son, Bone morphogenetic protein-7 inhibits vascular calcification induced by high vitamin D in mice, Tohoku J. Exp. Med. 221 (2010) 299–307, https://doi.org/10.1620/tjem.221.299.
[39] A. Bas, I. Lopez, J. Perez, M. Rodriguez, E. Aguilera-Tejero, Reversibility of calcitriol-induced medial artery calcification in rats with intact renal function, J. Bone Miner. Res. 21 (2006) 484–490, https://doi.org/10.1359/JBMR.051211.
[40] D.E. McMillan, Deterioration of the microcirculation in diabetes, Diabetes 24 (1975) 944–957, https://doi.org/10.2337/diab.24.10.944.
[41] D. Rizzoni, E. Porteri, D. Guelfi, M.L. Muiesan, U. Valentini, A. Cimino, E.A. Rosei, Structural alterations in subcutaneous small arteries of normotensive and hypertensive patients with non-insulin-dependent diabetes mellitus, Circulation 103 (2001) 1238–1244, https://doi.org/10.1161/01.CIR.103.9.1238.

Haigang Ma received his Ph.D. degree in MOE Key Laboratory of Laser Life Science and Institute of Laser Life Science at South China Normal University from 2014 to 2020. He is currently an associate professor of optical engineering, School of Electronic and Optical Engineering at Nanjing University of Science and Technology, China. His research interests are the development of novel biomedical imaging techniques including multifunctional photoacoustic microscopy, optical holography, and clinical photoacoustic/ultrasound imaging.

Yinshi Yu-master student from Nanjing University of Science and Technology. He is now in the third year of his master's degree and his current research focuses on applications of photoacoustic imaging in biomedicine.

Yahui Zhu- master student from Nanjing University of Science and Technology.

Hongjun Wu-Lecturer, currently pursuing a Ph.D. at Peking Union Medical College (Tsinghua University School of Medicine). He is engaged in fundamental and applied research in laser medicine, with a primary focus on the application of microscopic imaging in biomedicine to analyze the structure and function of organoids, organelles, and subcellular components.

Haixia Oiu is the director of the First Medical Center Laser medicine Department, deputy chief physician, master tutor. Her main research direction is the clinical application and mechanism study of photodynamic therapy in benign and malignant diseases, as well as the application of new optical technologies in precision diagnosis and treatment of photodynamic therapy. She is currently the executive editorial Board member of the Chinese Journal of Laser Medicine, the Standing Committee member of the Laser Medicine Branch of the Beijing Medical Association, the member of the board of directors of the Chinese Optical Society, and national natural science evaluation expert.

Ying Gu is an academician of the Chinese Academy of Sciences chief physician, professor, director of Laser Medicine Department of the First Medical Center of PLA General Hospital, Director of Laser Medicine Center of Hainan Hospital. Permanent member of the International Federation of Laser Medicine Chairman of the Chinese Medical Association Laser Medicine Branch, chairman of the Chinese Optical Society. She presided over the development of China's first laser medicine clinical technology operating standards and diagnosis and treatment guidelines.

Qian Chen as a leading expert in the National Key Discipline of "Optical Engineering" at Nanjing University of Science and Technology. As the primary contributor, he has won a second class State Technological Invention Award, a second-class State Scientific and Technological Progress Award and five first-class provincial and ministerial-level science and technology awards. As the first inventor, he has obtained 74 granted invention patents, 16 PCT international patents, and 6 U.S. patents. He has authored three books and 300+ SCI papers, among which 40+ have been featured on the cover. Currently, he serves as a Fellow and Executive Director of the Chinese Society Optical Engineering and Executive Director of the Chinese Institute of Electronics.

Chao Zuo is a professor in optical engineering, Nanjing University of Science and Technology (NJUST), China. He leads the Smart Computational Imaging Laboratory (SCILab: www.scilaboratory.com) at the School of Electronic and Optical Engineering, NJUST. He has long been engaged in the development of novel Computational Optical Imaging and Measurement technologies, with a focus on Phase Measuring Imaging Metrology such as Holographic Interferometric Microscopy, Noninterferometic Quantitative Phase Imaging(QPI), Fringe Projection Profilometry (FPP), and Structured Illumination Microscopy (SI). He has authored > 200 peer-reviewed publications in prestigious journals with over 17,000 citations.